Nanoscale

Accepted Manuscript

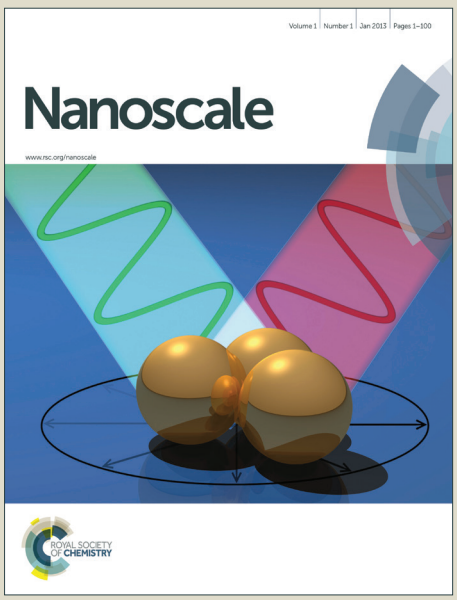

ROYAL SOCIETY OF CHEMISTRY

www.rsc.org/nanoscale

Journal Name

RSCPublishing

ARTICLE

Dynamic control of the location of nanoparticles in the hybrid co-assemblies

Cite this: DOI: 10.1039/x0xx00000x

Zhilong Su[a], Xiaokang Li[b], Xuesong Jiang*[a], Shaoliang Lin*[b], Jie Yin[a]

Received 00th January 2012,
Accepted 00th January 2012

DOI: 10.1039/x0xx00000x

www.rsc.org/

We herein demonstrated an approach to control the spatial distribution of component in the hybrid microsphere. The hybrid core-shell structured microsphere (CSM) prepared through co-assembly was used as starting material, which is comprised of anthracene-ended hyperbranched poly(ether amine) (AN-hPEA) in the shell and the crystallized anthracene containing polyhedral oligomer silsesquioxane (AN-POSS). Upon the thermal annealing at temperature higher than the melting point of AN-POSS, the diffusion of AN-POSS from the core to shell of CSM leads to a transition of morphology from the core-shell structure to core-transition-shell to the more stable homogeneous morphology, which has been revealed by experimental results of TEM and DSC. The mechanism for the morphology transition of CSM induced by the diffusion of AN-POSS was disclosed by a Dissipative Particle Dynamics (DPD) simulation. Mathematical model for the diffusion of POSS in the hybrid microsphere is established according to the Fick's law of diffusion and can be used to quantify its distribution in CSM. Thus the spatial distribution of POSS in microsphere can be controlled dynamically by tuning temperature and time of thermal annealing.

1. Introduction

Co-assembly of polymer and inorganic components provides a powerful bottom-up approach to construct the multi-functional hybrid materials with fancy properties.[1-6] Various hybrid co-assemblies were developed with the controllable morphologies including sphere[7, 8], cylindrical[9, 10], vesicles[11, 12], and other complex structures ranging from zero to three dimensions[13-15]. These assemblies have great potential application in many fields such as medical imaging, drug delivery, and catalysis as a result of the combination of the useful chemical and mechanical properties of polymer and the unique chemical, electronic, magnetic, and optical properties of inorganic component. Since the spatial distribution of the nanoparticles in hybrid materials is one of the critical factors to determine the properties of the obtained hybrid structure[16-18], many efforts have been made towards preparing the hybrid co-assemblies with the controllable location of inorganic component in polymer matrix.[19-23]

By varying precursor composition[24-27] or environmental parameters[28, 29] in co-assembly, various inorganic components such as nanoparticles (NPs) and nanorods have been located selectively in the different portion of the hybrid co-assemblies.[30, 31] Taton and co-workers[32] incorporated the oleic acid-coated magnetic NPs into the hydrophobic core of the spherical micelles of poly(styrene)-block-poly(acrylic acid) (PS-b-PAA). Eisenberg and co-worker[33] demonstrated a general approach for controlled incorporation of metal NPs into the central portion of vesicle wall, based on the NPs coated with the same block-polymer as vesicles. Through the similar approach, they also achieved the controlled location of NPs in the hydrophobic core of PS-b-PAA cylindrical micelles[34]. Park's group[9, 35] achieved the dense packing of magnetic NPs in the walls of polymer vesicles and demonstrated that the spatial arrangement of NPs in the polymer matrix can affect the magnetic relaxation rate of surrounding water. In these studies, the hydrophobic interaction, hydrogen bonding or electrostatic interactions, usually act as the driving forces for co-assembly of inorganic NPs and polymer, and the distribution of NPs in the resulting hybrid co-assemblies is controlled by the thermo-dynamic equilibrium.[23, 36-38] The arrangement of NPs in these researches is fixed during the process of co-assemble, and unchangeable after the formation of the hybrid co-assemblies, which means the static control of the location of NPs. Another possible and feasible way to control the location of NPs is to change the morphology of the resulted hybrid co-assemblies through post-treatment such as thermal or solvent annealing, which allows for the ability of tuning the location of NPs.[20, 36] To the best of our knowledge, however, the dynamic control of NPs' location in the hybrid co-assemblies is rarely reported.

We herein demonstrate the first example of the dynamic control of the distribution of NPs in the hybrid core-shell microspheres (CSM). The hybrid core-shell microspheres were prepared through co-assembly of amphiphilic hyperbranched poly(ether amine) (AN-hPEA) and polyhedral oligomeric

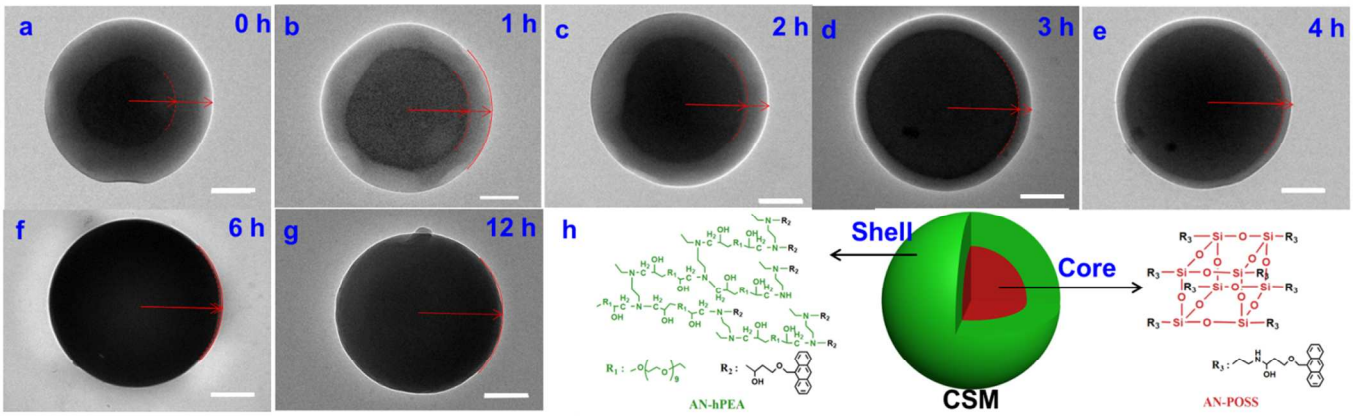

Figure 1. TEM tracing of CSM along thermal annealing at 85 °C for 0(a), 1(b), 2(c), 3(d), 4(e), 6(f), 12(g) hour(s). Scale bar 200 nm. (h) Chemical structure of AN-hPEA and AN-POSS.

silsesquioxanes (AN-POSS) NPs(Figure 1h).[39] This core-shell structured morphology is thermodynamically metastable, which was captured by the crystallized aggregation of POSS in the core during the co-assembly of AN-POSS and AN-hPEA. Upon thermal annealing, the diffusion of POSS from the core to the shell of AN-hPEA was observed, with this core-shell structure undergoing a transition to the thermodynamically more stable morphology with gradient distribution of POSS in the matrix of hPEA. During this process, the transitional state can be fixed by the cross-linking induced by photo-dimerization of anthracene[40], and the spatial distribution of POSS can be controlled dynamically by the temperature and time of thermal annealing. Particular attention was paid to the effect of diffusion in the confined geometry on the spatial distribution of POSS in the hybrid microsphere.

2. Results and discussion

2.1 Morphology transition upon thermal annealing

The hybrid core-shell microsphere (CSM) was prepared through co-assembly of amphiphilic AN-hPEA and hydrophobic AN-POSS NPs. Previous work of our group[39] revealed that the resulted hybrid CSMs prefer well-defined core-shell structure with low PdI of about 0.1, in which the core of the crystalized aggregation of AN-POSS is ~550 nm in diameter, and the hydrophilic shell of AN-hPEA is ~160 nm in thickness. In fact, the core-shell morphology of CSM is thermo-dynamically metastable, which is supported by the differential scanning calorimetry (DSC) results (Figure S1). The DSC thermo-gram of obtained CSMs shows a microphase-separated structure. However, the composites of AN-hPEA/AN-POSS with various ratios prepared by mixing in solution exhibit only one glass transition in DSC thermograms and no phase separation was observed after several heat-cool loops, indicating that these composites of AN-hPEA/AN-POSS are homogenous, and AN-hPEA & AN-POSS are completely compatible. In other words, AN-POSS can be dispersed in the polymer matrix of AN-hPEA in molecular scale. The outstanding compatibility between AN-hPEA and AN-POSS might be ascribed to the strong π-π interaction of anthracene moieties in AN-hPEA and AN-POSS. The DSC results revelled that the CSM is thermo-dynamically unstable and possible to transfer to homogenous structure under certain conditions. Thus we make the assumption that upon the thermal annealing at a temperature higher than the melting point of AN-POSS, the microphase separated core-shell structure may undergo a transition to a more stable homogeneous structure with the change of distribution of POSS NPs spontaneously.

The uniform-sized and well-defined core-shell structure provide the hybrid microsphere an idea model to study the migration of NPs in confined geometry in micro-scale. The morphology evolution of CSM on the thermal annealing at 85 °C in water was recorded by TEM images and the migration of POSS from the core to the shell of AN-hPEA was observed. As shown in Figure 1, the boundary between the core of AN-POSS (dark) and the shell of AN-hPEA can be observed before thermal annealing (0 h). Along the thermal annealing, the boundary shifts to the outside and the thickness of shell becomes thinner obviously, indicating the migration of AN-POSS from the core to the shell of AN-hPEA.

At 85 °C, a temperature higher than the melting point of AN-POSS (~65 °C, Figure 2a), the crystallization of AN-POSS in the core is destroyed and migration starts. Along thermal annealing, AN-POSS in the core gradually migrates into the shell of AN-hPEA to form the transition layer, and the core of AN-POSS becomes smaller. The dark area in CSM in TEM images (Figures 1b-1e) is comprised of the core of the crystallized AN-POSS and the transition layer composed of both AN-POSS and AN-hPEA. There is no obvious boundary between the core of POSS and the transition layer in TEM images, which might be explained by the electron density of POSS is much higher than AN-hPEA. After annealed at 85 °C for 6 h, the shell of AN-hPEA almost disappeared, indicating that AN-POSS diffuses to the edge of CSM (Figure 1f). Further thermal annealing leads the CSM to the more homogenous morphology (Figure 1g). Although the interior morphology

changes dramatically along the thermal annealing, the shape and size of the hybrid co-assemble keep almost unchanged, which was supported by SEM images and DLS results (Figure S2). This may ascribe to the fact that the hydration shell of CSM prevents it from fusing with each other. Moreover, cross-section TEM images of microsphere (Figure S3) were captured and the morphology transition from the microphase-separated core-shell to the homogeneous structure was further confirmed.

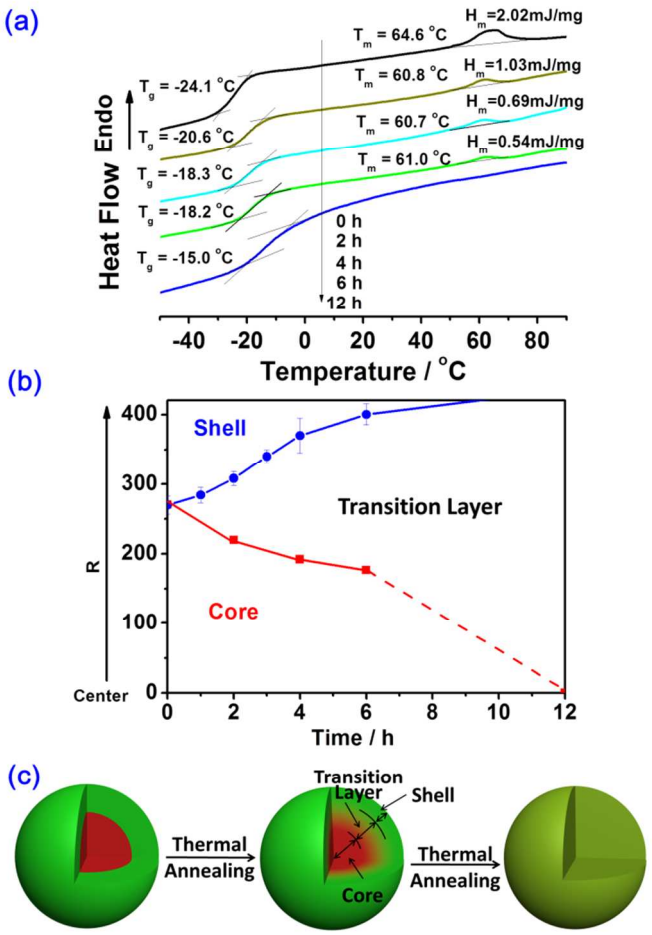

Figure 2. (a) DSC thermograms of CSM along thermal annealing at 85 °C for different time. (b) The dependence of radius of core (R_c), thickness of transition layer (T_t) and shell (T_s) of CSM on the thermal annealing at 85 °C. (c) The proposed scheme for the morphology transition of CSM along with thermal-annealing.

The morphology transition of the hybrid CSM along thermal annealing was also investigated by DSC. Figure 2(a) shows DSC thermograms of CSM annealed for different length of time. Before thermal annealing, the CSM exhibits an obvious glass transition of -24.1 °C (the shell of AN-hPEA) and a melting peak at around 65 °C (crystallized AN-POSS in the core). In comparison with the pure AN-POSS (Figure S1), the melting enthalpy (H_m) of CSM (2.02 mJ/mg) is around 1/3 of pure AN-POSS (6.20 mJ/mg), which is almost the same to the feed ratio of AN-POSS in CSM. This result reveals that almost all AN-POSS in feed prefers the crystallized aggregation in the core of CSM. Along the thermal annealing at 85 °C, the glass transition temperature (T_g) of the CSM increases, while melting point (T_m) and H_m shifts to the lower temperature slightly and decreases obviously, respectively. The increased T_g of CSM might be ascribed to the migration of AN-POSS from the core to the shell of AN-hPEA. Generally, the incorporation of inorganic nanoparticles of POSS can enhance T_g of the soft polymer matrix.[6] Simultaneously, the size of the crystallized core of AN-POSS becomes smaller due to the diffusion of AN-POSS from the core to the shell of AN-hPEA, resulting in the decrease of H_m. This also means that the POSS core remains during thermal annealing. In other words, the extended dark core in TEM images (Figures 1b-d) should be comprised of the smaller core of the crystallized AN-POSS and the transition layer composed of AN-POSS and AN-hPEA.

After 6 hours of thermal annealing, melting enthalpy (H_m) of the CSM decreases to 0.54 mJ/mg according to DSC (Figure 2a), indicates that the crystallized core still exists although AN-POSS has diffused to the surface and the pure AN-hPEA shell disappears (Figure 1e). After 6 hour of thermal annealing further (total 12 h), the melting peak disappears completely and only glass transition at -12 °C can be observed in the DSC thermograms. The T_g of CSM after 12 h thermal annealing is close to that of AN-POSS/AN-hPEA=1:2 composite (-9 °C, Figure S1), indicating that POSS NPs tend to disperse homogeneously in the hybrid CSMs after thermal annealing. The combination of TEM and DLS results can support the mechanism proposed in Figure 2c, which illustrates the morphology transition of CSMs along thermal annealing: core-shell to core-transition-shell to homogeneous.

After revealing the interior morphology of CSMs during thermal annealing, it is necessary to determine quantitatively the size of the crystallized AN-POSS core (R_c, radius), the thickness of transitional layer (T_t) comprised of both AN-POSS and AN-hPEA, and the thickness of the AN-hPEA shell (T_s). Since the obvious boundary between the transition layer and the shell can be observed in TEM images (Figure 1), T_s was determined directly by TEM. The size of the crystallized AN-POSS core can be estimated from the data of H_m shown in Figure 2(a). Generally, the melting enthalpy can be used to estimate the amount of crystallized component with the assumption that the materials keep a similar degree of crystallization after treatment. As H_m is proportional to the volume of the crystallized AN-POSS, $R_{c(t)}$ can be given as follows:

$$R_{c(t)} = R_{c(0)} \times \left(\frac{H_{m(t)}}{H_{m(0)}}\right)^{1/3} \quad (1)$$

where $R_{c(0)}$ and $H_{m(0)}$ are the radius and melting enthalpy of the crystallized AN-POSS core before the thermal annealing, respectively. The thickness of shell (T_s) and the radius of the crystallized core (R_c) dependent on time of thermal annealing are presented in Figure 2b. Based on the known T_s and R_c, and the almost unchanged size of the sphere of co-assemblies (Radius~435 nm, Figure S2), the thickness of the transitional layer (T_t) can be calculated according to the formula: T_t= 435nm - R_c - T_s. Figure 2(b) summarizes the obtained dates regarding to R_c, T_t, and T_s vs. *time* along thermal annealing.

Upon thermal annealing, the transition layer is generated and its thickness (T_t) increases with the time due to the diffusion of AN-POSS from core into the shell.

To fully understand the diffusion behaviour of AN-POSS in the confined geometry, the thermal annealing of CSM at various temperatures was carried out. As the core-shell morphology is kinetically trapped by the crystallized aggregation of AN-POSS, this thermodynamically metastable state is expected to keep stable when temperature is below the melting point of AN-POSS (65 °C). This is indeed true that CSM can keep the microphase-separated core-shell morphology at least for one month at room temperature. Even heating at 55 °C for 48 h, no obvious change was found in the size of the crystallized core and the shell of CSM (Figure 3c), which is in the contrast to the obvious morphology transition at 85 °C. This can be explained by the fact that the crystallization restricts the mobility of AN-POSS, resulting in no diffusion of AN-POSS from core to the shell of AN-hPEA. When the annealing temperature is higher than T_m (65 °C and 75 °C), CSM takes the similar morphology transition to that annealed at 85 °C, and the dark area of CSM in TEM images expands with the annealing time increasing (Figures 3a and 3b). The speed of dark core increment is obviously slower at the lower temperature. The shell of AN-hPEA disappeared after being heated at 75 °C for 48 h, while the shell with thickness of 75 nm can still be seen in TEM images even after thermal annealing at 65 °C for 48 h. The temperature dependence of CSM morphologic transition confirms that the migration of AN-POSS into the shell of AN-hPEA is controlled by the diffusion. The higher temperature can provide the higher molecular mobility, resulting in the faster diffusion of AN-POSS into the shell of AN-hPEA, and consequently quicker morphology transition.

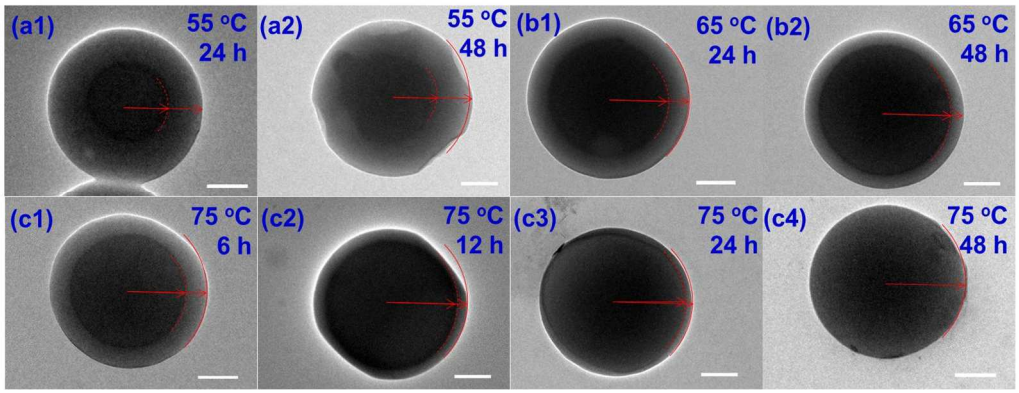

Figure 3. TEM images of CSM along thermal annealing at different temperatures (a) 55 °C; (b) 65 °C; (c) 75 °C. Scale bar 200 nm.

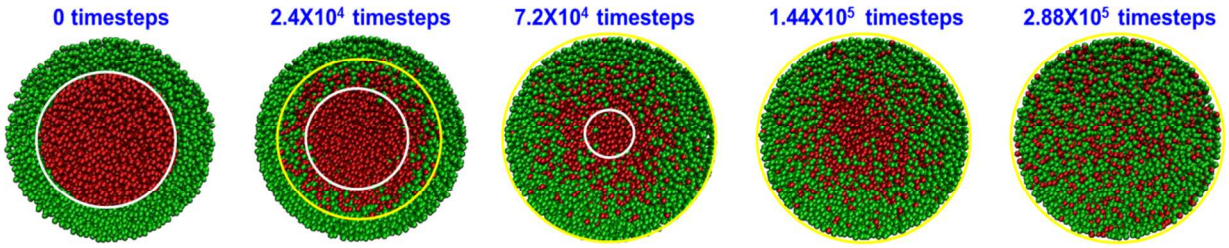

Figure 4. Simulated snapshots of CSM (section of the center) at various annealing times according DPD simulations, which show the morphology transition from a core-shell structure to a core-transition-shell structure and to a homogeneous structure. The green and red beads refer to AN-hPEA and AN-POSS, respectively. Corresponding spatial distribution of AN-POSS in CSM along the radius direction at different annealing timesteps are shown in figure S4. Note: $1.2x10^5$ timesteps corresponding to 1 hour of thermal annealing.

2.2 Dissipative Particle Dynamics (DPD) simulations

The above results reveal that the morphologies of hybrid microsphere changes with the diffusion of AN-POSS in a confined geometry during the annealing process. To give a clear view of the motion of nanoparticles, Dissipative Particle Dynamics (DPD) simulations[41, 42] was performed to investigate the structural evolution of CSM along the thermal annealing. A core-shell structured model before thermal-annealing (0 timesteps) was constructed (Figure 4, Scheme S1g), where AN-hPEA and AN-POSS were represented by green and red beads, respectively. The simulation details can be found in Supporting Information.

Figure 4 clearly presents the sectional views of five typical stages concerning simulated CSM morphologies during the thermal annealing process. During thermal annealing, AN-POSS nanoparticles (red beads) in the core diffuse into the shell of AN-hPEA (green beads) gradually, leading to the appearance of a transitional layer containing both AN-hPEA and AN-POSS. The thickness of the transitional layer is about 1/4 of the radius of CSM at $2.4x10^4$ timesteps (corresponding for 2 h annealing). The shell thickness decreases further as the

annealing time increases while the thickness of transitional layer increases. The shell of AN-hPEA almost disappears at $7.2\text{x}10^4$ timesteps (corresponding for 6 h annealing). When the annealing time is $2.88\text{x}10^5$ timesteps (corresponding for 24 h annealing), the CSM exhibits a near homogenous structure with AN-hPEA and AN-POSS mixed freely. The simulation results reproduce the general feature of the morphological transition of CSM upon thermal annealing. In addition, the simulations provide the spatial distribution information of AN-POSS in CSM, capturing more microscopic details of the CSM structure. Figure 4b shows the normalized density profiles of AN-POSS along the radius direction at various annealing times. The DPD results reflecting some characteristics of diffusion-controlled behaviour, and supported the proposed mechanism of structural evolution of CSM (Figure 2c).

2.3 Dynamical control of NPs' location in hybrid CSM

The spatial distribution in composition is of considerable interest in the design for new materials: the programmable materials, optical materials, and damping materials etc.[43-45] For example, because the continuously changing composition can minimize reflection at the interface of two materials, thus increasing the optical transmittance and enhancing resolution of optical materials.

Thus the control of the spatial distribution of nanoparticles in hybrid assemblies seems necessary. As the spatial distribution of POSS in CSM on thermal annealing shows some characteristics of diffusion, Fick's second law of diffusion[46, 47] (Equation 2) is used to predict the migration of AN-POSS from the core to shell of CSM.

$$\frac{\partial C}{\partial t} = D\frac{\partial^2 C}{\partial r^2} \qquad (2)$$

Where D, C, t and r are the diffusion constant, concentration, time and radial axis, respectively. Equation (2) can be expressed as follows[46]:

$$C_{(r)} = \frac{C_0}{2}\left\{\mathrm{erf}\left[\frac{(r_0-r)}{2\sqrt{D\cdot t}}\right] + \mathrm{erf}\left[\frac{(r_0+r)}{2\sqrt{D\cdot t}}\right]\right\} - \frac{\sqrt{\frac{D\cdot t}{\pi}}\left\{\exp\left[\frac{-(r_0-r)^2}{4\cdot D\cdot t}\right] - \exp\left[\frac{-(r_0+r)^2}{4\cdot D\cdot t}\right]\right\}}{r} \qquad (3)$$

Equation (3) gives the concentration of AN-POSS along the radial axis at different times of thermal annealing. C_0 is the concentration in the core of crystallized AN-POSS aggregation and can be regarded as 1.0 (100%). r_0 is the radius of the core, 275 nm. Based on the shell thickness of hybrid microsphere at the different time of thermal annealing determined by TEM, the diffusion constant (D) of AN-POSS in the shell of AN-hPEA at different temperatures can be calculated according to Equation (3). The diffusion constant (D) of AN-POSS at 85, 75, and 65 ^{o}C is 0.120, 0.038, and 0.009 nm^2/S, respectively. The diffusion constant is very low, and increases almost 13 times when the temperature increased from 65 to 85 ^{o}C. The low diffusion constant might be ascribed to the hydrodynamic volume of AN-POSS, which is much bigger than the low- molecular weight molecules, resulting in the less mobility and slower diffusion in the polymer matrix.

Figure S5 shows the linear Arrhenius plot, from which the diffusion activation energy (Q) is calculated to be 130.4 kJ/mol. The high diffusion activation energy might be also ascribed to the nature of AN-POSS as NPs. The spatial distribution of AN-POSS along the thermal annealing at 85 ^{o}C is further calculated according to equation (3) and shown in Figure 5, which reveals the detailed change of AN-POSS concentration along the axis with the time of thermal annealing. To simplify equation (3), the concentration of AN-POSS in the core and the shell is defined as 1.0 and 0, respectively. Due to the difference of concentration between core and shell, AN-POSS diffuses into the hPEA shell along the axis during the thermal annealing. The spatial distribution of AN-POSS changes fast at the beginning of thermal annealing, and turn slow in the later stage. This is the typical diffusion behaviour driven by the concentration difference. Before thermal annealing, the concentration of AN-POSS at the interface between the core and shell shows a sharp change from 1 to 0. Along thermal annealing, the transition layer generated and expanded into the whole CSM, in which the concentration of AN-POSS decreases gradually along axis. The further thermal annealing makes the concentration difference along axis smaller, leading to the more homogeneous morphology. Figure 5 predicts the concentration gradient of AN-POSS along axis in the transitional layer at different time of thermal annealing, which cannot be determined by TEM images of hybrid microsphere. The concentration gradient along axis decreases with the increasing time of thermal time. As shown in Figure 5, the core of the crystallized AN-POSS disappears after thermal annealing for 10 h, which is in agreement with the DSC results.

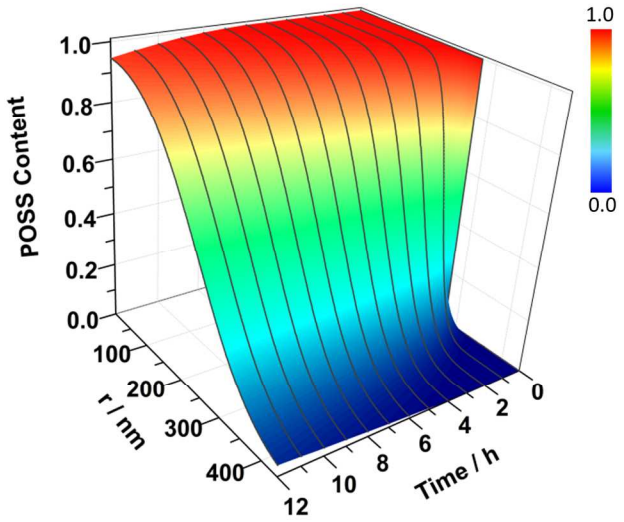

Figure 5. The spatial distribution of AN-POSS in hybrid microsphere along the radius at different annealing times, which is calculated from the Fick's second law (annealing temperature is 85 ^{o}C).

To verify the feasibility of this strategy for the dynamical control of NPs' location, another core-shell hybrid co-assembly of AN-POSS/ AN-hPEA=1/1 was also annealed thermally at 85

°C(Figure 68). They undergo the same morphology transition from the core-shell to core-transition-shell to homogeneous structure (Figure 6). Equation 3 was utilized to predict the distribution of AN-POSS NPs in CSM-2. Substitute the variables (D=0.120 nm^2/s; r_0= 351 nm; r=1,2...466) into the equation3, gives the distribution AN-POSS NPs in CSM-2. Both predicted shell thickness and experimental data were summarized in Table1. The predicted data meet with experimental data well, indicating the feasibility of controlling the distribution of NPs in CSMs.

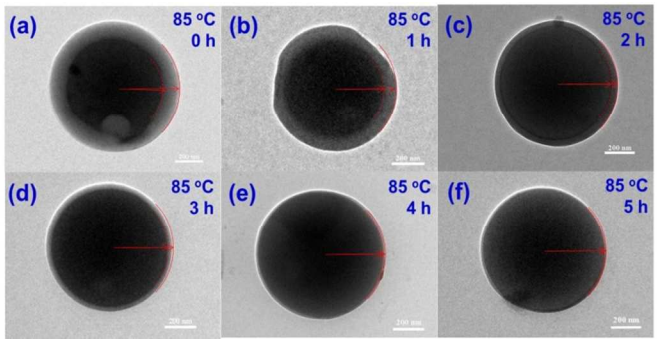

Figure 6. TEM images of CSM-2 (AN-hPEA/AN-POSS=1/1) upon different annealing time (85 °C). Scale bar 200 nm.

Table1. Shell thickness (T_s) of CSM-2 upon different annealing time (85 °C).

Annealing time(h)	0	1	2	3	4	5
Predicted (nm)		69	51	38	27	18
Experimental(nm)	115	78	50	38	17	10

Furthermore, the transition state of CSM can be fixed by the cross-linking induced by photo-dimerization of anthracene[40]. After exposure of 365 nm UV-light for 15 min the dimerization degree of AN groups is around 75 % (Figures S5a,b).The morphology remains well in tetrahydrofuran (THF) solution, suggesting that the whole microsphere is cross-linked tightly (Figure S6c). Even under the further thermal annealing at 85 °C, the cross-linked temporary morphology does not exhibit any obvious change (Figures S5d and e). This can be explained by that the cross-linking *via* dimerization of AN moieties freezes the mobility of AN-POSS and AN-hPEA, leading to no diffusion of AN-POSS from the core to the shell. Therefore, combination of the thermal annealing and photo-cross-linking provide an approach to dynamic control of the spatial distribution of AN-POSS in these hybrid co-assemblies.

2.4 Mechanical performance of hybrid gradient microsphere

AFM is powerful to detect the mechanical properties of materials with nano-scale, and provide some insights into the fine details of polymer surfaces and interfaces.[48-50] Force curve measurements are carried out by AFM to assess the mechanical properties of the annealed hybrid microsphere: the sample is compressed by the indenting AFM tip and the elastic response of the sample under this loading force is analyzed. Young's modulus (E) is calculated from the force curves using the Hertz model. To enhance the stability, the annealed hybrid microsphere is cross-linked by irradiation of 365 nm UV-light before AFM measurement.

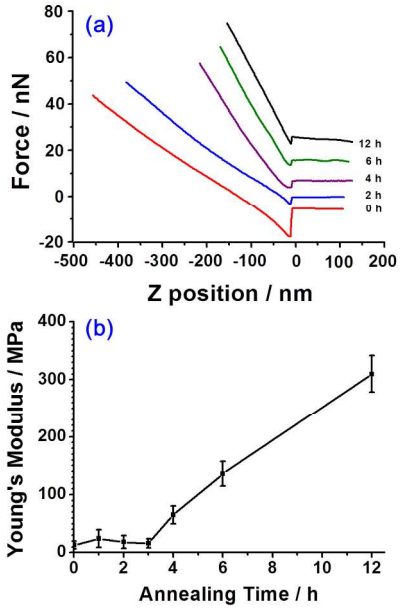

Figure 7. Typical force curves (a) and the Young's modulus (b) of hybrid microsphere annealed at 85 °C for different time.

Figure 7a shows the representative force curves along thermal annealing at 85 °C. Since the diameter of the hybrid microsphere in this study is over 800 nm, the fitting analysis range is z = 0 - 60 nm (i.e., less than 10 % of the CSM height) of the force curves to determine E values. Figure 7b presents E values at various annealing time which are calculated by averaging multiple probing points. The Young's modulus is 12 MPa before thermal annealing and remains almost unchanged along thermal annealing for the first 3h, which is comparable to 13 MPa of the pure AN-hPEA matrix (Figure S7). This confirms that the hybrid microsphere is covered by the thick shell of AN-hPEA even after thermal annealing for 3h, which is in good agreement with the results of TEM. After annealed for 4h, the Young's modulus increases to 75 MPa although the hybrid microsphere at this stage still keeps the core-transition layer-shell structure. This might be explained by that the transitional layer can act as the substrate to influence E value [51]. In other words, the E value of 75 MPa determined by AFM results from both the shell and transitional layer. Generally, the incorporation of POSS nanoparticles can enhance the mechanical properties of polymer matrix such as modulus and hardness. The enhanced E value of CSM should be ascribed to the increasing concentration of AN-POSS nearby the surface of hybrid microsphere, resulting from the diffusion of AN-POSS from the center to surface. After annealed for 12 h, the Young's modulus increases to 310 MPa, in the same order of magnitude to that of the AN-POSS/AN-hPEA composite (Figure S6, POSS content 0.33, 410 MPa). This indicates that the

concentration of AN-POSS nearby the surface of CSM increases and the distribution of AN-POSS in the hybrid microsphere turns more homogeneous along the thermal annealing. These results of the measurement of AFM force curves can be well explained by the morphology transition, which revealed by both experimental results of TEM and theory stimulation.

3. Experimental Section

3.1 Preparation of core-shell microspheres (CSM) and their thermal annealing

The preparation of core-shell microspheres was discussed in detail in our previous work.[39] Typically, 6.6 mg of AN-hPEA and 3.3 mg of AN-POSS were first dissolved into 1 mL of dioxane, which is a good solvent for both AN-hPEA and AN-POSS. The solution equilibrated at 25 ^{o}C for 1 hour before 9 mL of mili-Q water was added slowly to the solution (5 mL of water per hour). The polymer solution was gently stirred during the water addition process. Then, the samples were dialyzed against water for 24 h and collected for further treatment. The CSM described in this paper is not cross-linked unless specifically noted.

In a typical annealing process, 10 ml of CSM aqueous solution (1 mg/ml) was filled in a 25 ml bottle. Then the CSM aqueous solution was placed in a precisely controlled heater (IKA RET Basic equipped with ETS-D5, Germany) under a gentle stir.

4. Conclusion

In summary, the spatial distribution of POSS in the hybrid microsphere can be predicted and controlled dynamically through diffusion approach. The hybrid core-shell microsphere (CSM) prepared by co-assembly of AN-POSS and AN-hPEA was taken as a model, in which the shell is comprised of AN-hPEA and the core is comprised of the crystallized aggregation of AN-POSS. Upon the thermal annealing at temperature higher than the melting point of AN-POSS, the diffusion of AN-POSS from the core to shell of CSM leads to a transition of morphology from the core-shell structure to core-transition-shell to the thermodynamically more stable homogeneous morphology, which was confirmed by experimental results of TEM and DSC, theory calculation of Fick's second law of diffusion and DPD simulation. During this process, the location of POSS in CSM can be controlled dynamically by the temperature and time of thermal annealing. AFM force curves revealed that the spatial distribution of POSS nanoparticles generates significant influence on the mechanical properties of CSM. Generally, for a phase-separated system with two compatible component, this process can be used to fabricate hybrid materials with controlled location of nanoparticles in micro-assemblies including Core-Shell Sphere and other heterogeneous structure trapped by kinetics. We believe that this concept for the dynamical control of nanoparticle's location by diffusion can provide some new guidelines in designing and preparing the hybrid co-assemblies with the desired functions and properties.

Acknowledgements

The authors thank the National Nature Science Foundation of China (21174085, 21274088, 51373098), Education Commission of Shanghai Municipal Government (12ZZ020) for their financial support. We also thank Prof. Z. H. Luo for his helpful discussion on the diffusion equation. X. J. is supported by the NCET-12-3050 Project.

Notes and references

[a] School of Chemistry & Chemical Engineering, State Key Laboratory for Metal Matrix Composite Materials, Shanghai Jiao Tong University. 800 Dongchuan Rd. Shanghai 200240, China.
E-mail: ponygle@sjtu.edu.cn
[b] School of Materials Science and Engineering, East China University of Science and Technology,
130 Meilong Rd. Shanghai 200237, China
E-mail: slin@ecust.edu.cn

† Electronic Supplementary Information (ESI) available: Experimental details; Additional TEM images; DPD method. See DOI: 10.1039/c000000x/

1. A. C. Balazs, T. Emrick and T. P. Russell, *Science*, 2006, **314**, 1107-1110.
2. A. H. Lu, E. L. Salabas and F. Schuth, *Angew. Chem., Int. Ed.*, 2007, **46**, 1222-1244.
3. M. C. Daniel and D. Astruc, *Chem. Rev.*, 2004, **104**, 293-346.
4. M. C. Orilall and U. Wiesner, *Chem. Soc. Rev.*, 2011, **40**, 520-535.
5. Z. Nie, A. Petukhova and E. Kumacheva, *Nat Nano*, 2010, **5**, 15-25.
6. W. A. Zhang and A. H. E. Muller, *Prog. Polym. Sci.*, 2013, **38**, 1121-1162.
7. B. Yan, J.-C. Boyer, N. R. Branda and Y. Zhao, *Journal of the American Chemical Society*, 2011, **133**, 19714-19717.
8. J.-F. Berret, N. Schonbeck, F. Gazeau, D. El Kharrat, O. Sandre, A. Vacher and M. Airiau, *J. Am. Chem. Soc.*, 2006, **128**, 1755-1761.
9. Q. Luo, R. J. Hickey and S.-J. Park, *ACS Macro Lett.*, 2013, **2**, 107-111.
10. J. Y. Yuan and A. H. E. Muller, *Polymer*, 2010, **51**, 4015-4036.
11. C. Sanson, O. Diou, J. Thévenot, E. Ibarboure, A. Soum, A. Brûlet, S. Miraux, E. Thiaudière, S. Tan, A. Brisson, V. Dupuis, O. Sandre and S. Lecommandoux, *ACS Nano*, 2011, **5**, 1122-1140.
12. M. R. Rasch, E. Rossinyol, J. L. Hueso, B. W. Goodfellow, J. Arbiol and B. A. Korgel, *Nano Lett.*, 2010, **10**, 3733-3739.
13. Y. Guo, S. Harirchian-Saei, C. M. S. Izumi and M. G. Moffitt, *ACS Nano*, 2011, **5**, 3309-3318.

14. M. S. Nikolic, C. Olsson, A. Salcher, A. Kornowski, A. Rank, R. Schubert, A. Frömsdorf, H. Weller and S. Förster, *Angew. Chem., Int. Ed.*, 2009, **48**, 2752-2754.
15. M. R. Bockstaller, R. A. Mickiewicz and E. L. Thomas, *Adv. Mater.*, 2005, **17**, 1331-1349.
16. E. González, J. Arbiol and V. F. Puntes, *Science*, 2011, **334**, 1377-1380.
17. Y. Yin and A. P. Alivisatos, *Nature*, 2005, **437**, 664-670.
18. S. Liu, Z. Sun, Q. Liu, L. Wu, Y. Huang, T. Yao, J. Zhang, T. Hu, M. Ge, F. Hu, Z. Xie, G. Pan and S. Wei, *ACS Nano*, 2014, **8**, 1886-1892.
19. Y. Mai and A. Eisenberg, *Acc. Chem. Res.*, 2012, **45**, 1657-1666.
20. S. G. Jang, D. J. Audus, D. Klinger, D. V. Krogstad, B. J. Kim, A. Cameron, S.-W. Kim, K. T. Delaney, S.-M. Hur, K. L. Killops, G. H. Fredrickson, E. J. Kramer and C. J. Hawker, *J. Am. Chem. Soc.*, 2013, **135**, 6649-6657.
21. T. Chen, M. Yang, X. Wang, L. H. Tan and H. Chen, *J. Am. Chem. Soc.*, 2008, **130**, 11858-11859.
22. B. L. Sanchez-Gaytan, W. Cui, Y. Kim, M. A. Mendez-Polanco, T. V. Duncan, M. Fryd, B. B. Wayland and S.-J. Park, *Angew. Chem., Int. Ed.*, 2007, **46**, 9235-9238.
23. W. Li, S. Liu, R. Deng and J. Zhu, *Angew. Chem., Int. Ed.*, 2011, **50**, 5865-5868.
24. R. J. Hickey, J. Koski, X. Meng, R. A. Riggleman, P. Zhang and S.-J. Park, *ACS Nano*, 2013, **8**, 495-502.
25. J. J. Chiu, B. J. Kim, E. J. Kramer and D. J. Pine, *J. Am. Chem. Soc.*, 2005, **127**, 5036-5037.
26. L. H. Tan, H. Xing, H. Chen and Y. Lu, *J. Am. Chem. Soc.*, 2013, **135**, 17675-17678.
27. L. Zhang, J. Lin and S. Lin, *Macromolecules*, 2007, **40**, 5582-5592.
28. X. Yu, S. Zhong, X. Li, Y. Tu, S. Yang, R. M. Van Horn, C. Ni, D. J. Pochan, R. P. Quirk, C. Wesdemiotis, W.-B. Zhang and S. Z. D. Cheng, *J. Am. Chem. Soc.*, 2010, **132**, 16741-16744.
29. S. G. Jang, B. J. Kim, C. J. Hawker and E. J. Kramer, *Macromolecules*, 2011, **44**, 9366-9373.
30. A. Walther and A. H. E. Müller, *Chem. Rev.*, 2013, **113**, 5194-5261.
31. A. H. Groschel, A. Walther, T. I. Lobling, F. H. Schacher, H. Schmalz and A. H. E. Muller, *Nature*, 2013, **503**, 247-251.
32. B.-S. Kim, J.-M. Qiu, J.-P. Wang and T. A. Taton, *Nano Lett.*, 2005, **5**, 1987-1991.
33. Y. Mai and A. Eisenberg, *J. Am. Chem. Soc.*, 2010, **132**, 10078-10084.
34. Y. Mai and A. Eisenberg, *Macromolecules*, 2011, **44**, 3179-3183.
35. R. J. Hickey, A. S. Haynes, J. M. Kikkawa and S.-J. Park, *J. Am. Chem. Soc.*, 2011, **133**, 1517-1525.
36. S. G. Jang, A. Khan, C. J. Hawker and E. J. Kramer, *Macromolecules*, 2012, **45**, 1553-1561.
37. R. J. Hickey, Q. Luo and S.-J. Park, *ACS Macro Lett.*, 2013, **2**, 805-808.
38. S. Yang, C.-F. Wang and S. Chen, *J. Am. Chem. Soc.*, 2011, **133**, 8412-8415.
39. Z. Su, B. Yu, X. Jiang and J. Yin, *Macromolecules*, 2013, **46**, 3519-3528.
40. B. Yu, X. S. Jiang and J. Yin, *Soft Matt.*, 2011, **7**, 6853-6862.
41. Y.-J. Sheng, C.-H. Nung and H.-K. Tsao, *J. Phys. Chem. B*, 2006, **110**, 21643-21650.
42. Y. Xu, J. Feng, H. Liu and Y. Hu, *Mol. Simul.*, 2008, **34**, 559-565.
43. Y. Liu, M. Takafuji, H. Ihara, M. Zhu, M. Yang, K. Gu and W. Guo, *Soft Matt.*, 2012, **8**, 3295-3299.
44. N. Zhao, Z. Wang, C. Cai, H. Shen, F. Liang, D. Wang, C. Wang, T. Zhu, J. Guo, Y. Wang, X. Liu, C. Duan, H. Wang, Y. Mao, X. Jia, H. Dong, X. Zhang and J. Xu, *Advanced Materials*, 2014, **26**, 6994-7017.
45. T. Konig, P. Ledin, M. Russell, J. Geldmeyer, M. Mahmoud, M. A. El-Sayed and V. V. Tsukruk, *Nanoscale*, 2015, 10.1039/C1034NR06430E
46. J. Crank, *The Mathematics of Diffusion*, Oxford University Press, 1979.
47. F. D. Fischer and J. Svoboda, *Prog. Mater. Sci.*, 2014, **60**, 338-367.
48. M. E. McConney, S. Singamaneni and V. V. Tsukruk, *Polym. Rev.*, 2010, **50**, 235-286.
49. H. Y. Yoshikawa, F. F. Rossetti, S. Kaufmann, T. Kaindl, J. Madsen, U. Engel, A. L. Lewis, S. P. Armes and M. Tanaka, *J. Am. Chem. Soc.*, 2011, **133**, 1367-1374.
50. H. Liu, N. Chen, S. Fujinami, D. Louzguine-Luzgin, K. Nakajima and T. Nishi, *Macromolecules*, 2012, **45**, 8770-8779.
51. J. Domke and M. Radmacher, *Langmuir*, 1998, **14**, 3320-3325.